Galileo Photopolarimeter-Radiometer Observations of Jupiter and the Galilean Satellites

G. S. Orton, J. R. Spencer, L. D. Travis, T. Z. Martin, L. K. Tamppari

Photopolarimeter-Radiometer (PPR) maps of daytime temperatures on Ganymede at a resolution of 220 kilometers show the expected anticorrelation with albedo, but morning temperatures were about 10 kelvin warmer than expected. Europa had a subsolar temperature of 128 kelvin and a lower effective thermal inertia than either Ganymede or Callisto, and Io's night side was cooler than predicted by recent models, perhaps requiring revision of heat-flow estimates. The lowest 250-millibar temperatures in the Great Red Spot (GRS) generally corresponded to the visually darkest regions. Temperatures remained cold north of the GRS, but they rose by as much as 6 kelvin to the south over the 2800-kilometer PPR resolution. A visually bright region northwest of the GRS was also relatively cold. It is likely that NH_3 clouds affected the determination of the 500-millibar temperature field, which appears qualitatively different.

The Galileo Photopolarimeter-Radiometer (PPR) experiment was designed to cover a broad wavelength range (410 nm to >45 μm) in order to (i) produce a synoptic set of measurements on properties of cloud particles, temperature variations, and the local radiation budget in Jupiter and (ii) provide information on satellite surface characteristics (*1*). Here we present measurements of thermal infrared radiometric properties of the satellites and Jupiter made during the first encounter of the primary orbital mission.

We mapped the 17-μm brightness temperatures over the morning and midday portions of Ganymede's southern hemisphere (Fig. 1) with 200-km (~4.5° latitude) spatial resolution, which is better than the 500-km resolution of Voyager IRIS thermal maps (*2*). A strong anticorrelation between albedo and temperature is evident, as was seen at lower spatial resolution by Voyager. The magnitude of the temperature variations is roughly consistent with the variation in absorbed sunlight, for the assumption that surface thermal inertia is constant with albedo. There do not appear to be any locations where temperature varies independently of albedo. The maximum brightness temperature is 152 K, shortly after noon in the equatorial portions of Galileo Regio, compared to the maximum Voyager IRIS 17-μm brightness temperatures on this hemisphere of Ganymede of 149 K (*2*). This small discrepancy can be accounted for by the lower albedo of the region at the subsolar point and Ganymede's slightly smaller heliocentric distance compared with the Voyager observations. Voyager observed the afternoon cooling curve only; the PPR map includes the morning heating curve. Morning temperatures are more than 10 K warmer than predicted by one-layer, two-layer, and two-component models fitted to Voyager data and ground-based eclipse cooling data (*2*), so substantial revision of our understanding of Ganymede's thermal properties will probably be necessary.

The PPR measured the subsolar temperature on Europa. Observations at 37 μm along a 400-km (15° wide) strip give a subsolar brightness temperature of 128 K, which, when combined with Voyager 2 observations of the equatorial evening terminator temperature (about 90 K), can be fit with a homogeneous thermophysical model with a bolometric albedo of 0.63 and a thermal inertia of 2.6×10^4 erg cm^{-2} $s^{-1/2}$ K^{-1}. Although the homogeneous model ignores probable vertical and horizontal variations of thermal properties as well as subsurface sunlight penetration (*4*), it does allow comparison with the other icy Galilean satellites, which have significantly higher homogeneous-model thermal inertias: 7×10^4 for Ganymede and 5×10^4 for Callisto, as derived from Voyager data (*2*). This unusually low thermal inertia may be related to the unusually high regolith porosity inferred from photometry of Europa (*5*).

The PPR data included a global observation of Io's nightside thermal emission. Equatorial trailing-side 37-μm brightness temperatures at a local time near 9:00 PM, averaged over the 1600-km (50°) field of view, are between 80 and 85 K. This range is consistent with Voyager observations of smaller regions on the nightside (*6*). However, volcanic heat flow estimates by Veeder *et al.* (*7*) assumed that 80% of Io's surface had a diurnally constant temperature of about 109 K. This assumption would give a much higher nighttime 37-μm brightness temperature of 101 K, for an emissivity of 0.9, plus an additional substantial contribution from the hot spots. The low nighttime thermal emission suggests that more of the absorbed sunlight is reradiated from the day side, and thus, less of the dayside emission is attributable to volcanic heat than was assumed by Veeder *et al.* Estimates of volcanic heat flow may thus require revision.

The relative length of the initial encounter period enabled the Great Red Spot (GRS) to be mapped, in a strategy that

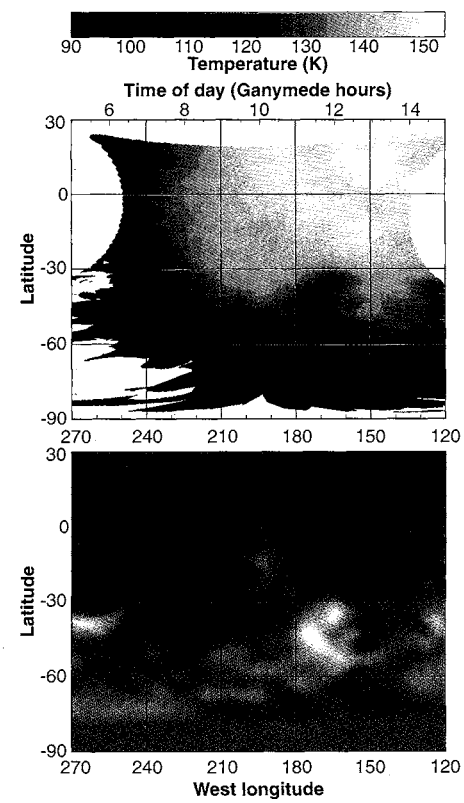

Fig. 1. False color representation of 17-μm daytime brightness temperatures on Ganymede (**top**) compared with albedo patterns derived from Voyager images (*3*) (**bottom**), smoothed to similar spatial resolution. Local time of day is given in the scale at the top: 12 "Ganymede hours" corresponds to local noon. The anticorrelation of temperature and albedo is clearly seen. Streaky structure in the lower left of the temperature map is an artifact. Steps in the temperature scale are at 2 K intervals.

G. S. Orton and T. Z. Martin, M.S. 169-237, Jet Propulsion Laboratory, California Institute of Technology, 4800 Oak Grove Drive, Pasadena, CA 91109, USA.
J. R. Spencer, Lowell Observatory, 1400 Mars Hill Road, Flagstaff, AZ 86001, USA.
L. D. Travis, Institute for Space Studies, NASA/Goddard Space Flight Center, 2880 Broadway, New York, NY 10025, USA.
L. K. Tamppari, M.S. 264-723, Jet Propulsion Laboratory, California Institute of Technology, 4800 Oak Grove Drive, Pasadena, CA 91109, USA.

coordinated synoptic observations by all four remote sensing instruments. The PPR derived the tropospheric temperature field of the GRS and vicinity. The temperature sounding experiment uses four discrete filters whose effective wavelengths are about 15, 22, 25, and 37 μm (660, 450, 405, and 270 cm^{-1}) (*1*). At these wavelengths, the opacity of the atmosphere is dominated by the collision-induced absorption of H_2. Because H_2 is well mixed, the outgoing thermal radiance can be inverted to retrieve the kinetic temperature field. The filter selection provided as wide of a vertical range of atmospheric sampling as possible; the peak of the outgoing thermal radiation in each channel varied from 200- through 700-mbar total pressure (*8*). The 250-mbar temperature field was determined largely by the measured radiance fields at 15, 22, and 25 μm, and the 500-mbar temperature field was determined largely by the measured radiances at 22 and 37 μm. The ~2800-km (2.2° longitude) diameter fields of view resolve the GRS about two times better than the Voyager IRIS zonal and meridional scans (*9*, *10*), about the same as the Voyager IRIS map of its interior (*9*), and about two times better than diffraction-limited ground-based telescopes such as the 3-m NASA Infrared Telescope Facility near 20 μm (*11*).

The 250-mbar map (Fig. 2) shows that the GRS is cold with respect to its surroundings. The coldest temperatures in the center are about 111 ± 1 K; variations do not exceed the expected measurement uncertainties. This temperature minimum area is confined to 314° to 328°W longitude. To the east and west, temperatures rise to ~114 ± 1 K in a broad axisymmetric region (~14° to 23°S) known as the South Tropical Zone (STrZ). The location of the steepest zonal (east-west) thermal gradient corresponds to the innermost dark area of the 410-nm image of the GRS (Fig. 2). To the north of this dark area, however, temperatures remain as cold as at the center, although over a narrower longitude range of 318° to 324°W. To the south, on the other hand, temperatures rise to 117 ± 1 K; the steepest gradient is no farther south than 37°S and just north of the visually dark ring surrounding the GRS. Relatively warm (118 to 120 K) temperatures are apparent east of 308°W longitude and north of 14°S latitude, and the warmest temperatures (119 to 122 K) are west of 338°W and north of 12°S in the extended region map. These are both generally coincident with visually dark areas associated with the broad axisymmetric region (~8° to 14° S) known as the South Equatorial Belt (SEB). The region south of 14°S in the map of the extended area, is cooler, with temperatures of 117 to 119 K, and it is more coincident with the lighter area in the 410-nm map. These temperatures are generally consistent with those derived from the Voyager IRIS data [figure 10 of (*9*)], although the temperature variations derived by Voyager IRIS are more symmetric in the meridional (north-south) direction.

The 500-mbar map (Fig. 2) is both similar to and different from the 250-mbar map. The coldest region in the center of the GRS is 128 ± 1 K, but it is surrounded by a warmer ring of 132 to 136 K located just to the exterior of the boundary of the steepest 250-mbar temperature gradients (except in the north). Exterior to this ring to the east, west, and south, temperatures are an intermediate 127 to 131 K. The region north of 12°S latitude and east of 308°W longitude, which is relatively warm at 250 mbar, is also a warm 132 to 136 K. Unlike temperatures at 250 mbar, the entire extended region west of 335°W longitude appears to be the warmest at 132 to 139 K. The 500-mbar temperature differences between the interior and exterior of the GRS are generally consistent with those derived from Voyager IRIS data (*10*). The bright ring around the GRS has the same morphology as the cloud-sensitive 5-μm emission observed by NIMS (*12*). This coincidence leads us to suspect that the variable optical thickness of an NH_3 condensate cloud influenced the upwelling radiance measured at 22 and 37 μm, where brighter radiances indicate relatively clearer regions of the atmosphere. If the 500-mbar temperature field were uniform, then the optical thickness of a vertically thin NH_3 condensate cloud near 600 mbar pressure would need to increase by a value of ~10 to match the mean observed 37-μm upwelling radiance. Accurate temperature sounding at this depth will require independent constraints on the cloud opacity, from NIMS data, from the PPR 45-μm cut-on filter measurements, or from ground-based NH_3 cloud-sensitive observations near 8.6 μm.

This observed temperature and cloud morphology are consistent with a model of the GRS as an anticyclonic vortex. High clouds and adiabatic cooling are associated with upwelling (*9*, *10*), and subsidence takes place at the immediate edge. Such a subsidence is consistent with the sudden rise in temperature and the appearance of an annulus of bright radiance at cloud-sensitive wavelengths which denotes a relative clearing in the cloud deck. Just as for the GRS itself, if one assumes that departures from constant temperatures along isobars are proportional to vertical winds, then the relatively cold 250-mbar temperatures north of the GRS that interrupt the normally warm SEB north of 12°N may indicate that the areas bright at 410 nm (Fig. 2) are regions of upwelling. By implication, these bright areas may be at

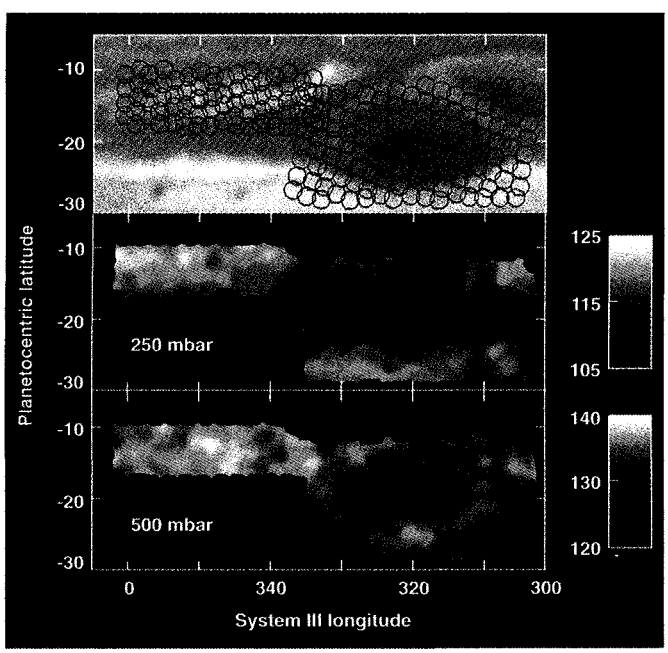

Fig. 2. Maps of upper tropospheric temperatures at the Great Red Spot and vicinity at 250 (**middle**) and 500 mbar (**bottom**). The region to the northwest was made in a separate observation sequence. Two separate shading schemes are used in order to enhance the observability of detail. The maps were made from a regular raster scanning pattern. (**top**) The pattern for the 22-μm filter on a reference background provided by a 410-nm map of the same region created from a synoptic observation by the Hubble Space Telescope Wide Field camera provided by K. Rages. The fields of view from the different filters were not coincident with one another. The value of a radiance measurement was assumed for the entire region covered by the instrument field of view. Unlike the satellite maps, the large Great Red Spot area was not sampled with highly overlapping fields of view. Radiance in areas not covered by adjacent fields of view was interpolated. The area from which temperatures were derived is slightly smaller than the field of view map shown because coverage by all filters was required.

least partly composed of higher altitude particles than their darker surroundings. If this interpretation is correct, then the 500-mbar maps show little sensitivity to the presence of these clouds in the field to the west of the GRS (longitudes to the west of 335°W), either because the upwelling is weak and the 500-mbar temperature difference is too small to measure or because the particles in these clouds are so small as to be ineffective in scattering or absorbing the 22- and 37-μm radiation from which the 500-mbar temperatures are largely derived. However, exceptions to the correlation between visually bright and thermally cool areas abound, including the locally dark STrZ, which is relatively cool, or the visually bright region south of the GRS, a part of which is relatively warm. It is clear that substantial revision will be required of the simple paradigm that regions of upwelling, cold air are associated with saturated gas–producing bright condensate particles.

The GRS temperature field will be further constrained by PPR G1 observations made at high emission angles, which have not yet been completely reduced. Further elucidation of the relationships between the temperature field, circulation, and cloud properties will also be made using maps of nearly all longitudes over a narrow latitude strip just north of the equator (*13*).

REFERENCES AND NOTES

1. E. E. Russell *et al.*, *Space Sci. Rev.* **60**, 531 (1992); Fig. 2 illustrates the bandpasses of the discrete filters compared with a spectrum of Jupiter.
2. J. Spencer, thesis, University of Arizona (1987); M. Urquhart and B. Jakosky, *J. Geophys. Res.* **101**, 21169 (1996).
3. New global controlled mosaic of Voyager Ganymede images prepared by R. Sucharski, (U.S. Geological Survey, Flagstaff, AZ).
4. R. H. Brown and D. L. Matson, *Icarus* **72**, 84 (1987).
5. D. L. Domingue, B. W. Hapke, G. W. Lockwood, D. T. Thompson, *Icarus* **90**, 30 (1991).
6. A. S. McEwen, in preparation.
7. G. J. Veeder, D. L. Matson, T. V. Johnson, D. L. Blaney, J. D. Goguen, *J. Geophys. Res.* **99**, 17095 (1994).
8. The recovery of temperatures uses the weighted-Chahine method [M. T. Chahine, *J. Atmos. Sci.* **27**, 960 (1970)] with additional weighting between the different filters according to their signal-to-noise ratios. The 1σ equivalent δT = 1.3 K for the 15-μm channel, 1.4 K for the 22-μm channel, 0.8 K for the 25-μm channel, and 1.6 K for the 37-μm channel, assuming average atmospheric radiances and averages of four samples for the channels at 15, 22, and 25 μm and 16 samples for the 37-μm channel, corresponding to the observing sequence used for the data reported here. In the radiative transfer model, the He mixing ratio of 13.6% reported by von Zahn and Hunten [*Science* **272**, 849 (1996)] was used, as was a value for the fraction of *para*-H_2 of 0.31 taken from Sada *et al.* (*9*).
9. P. V. Sada, R. F. Beebe, B. J. Conrath, *Icarus* **119**, 311 (1996).
10. F. M. Flasar, B. J. Conrath, J. A. Pirraglia, *J. Geophys. Res.* **86**, 8759 (1981).
11. G. S. Orton *et al.*, *Science* **265**, 625 (1994).
12. R. Carlson *et al.*, *ibid.* **274**, 385 (1996).
13. Not long after the start of these extensive observations, the PPR filter wheel was found to have remained at the position corresponding to the 37-μm discrete filter, despite commands to move to other filter positions. Therefore all subsequent measurements, including almost all the longitudes of this sequence, were made in the 37-μm discrete filter. Interpretation of these data without independent constraints on cloud properties will be challenging. Our G1 calibration target observations were also made only with this filter, which will make difficult our reexamination of the radiometric calibration.

14. We thank the Galileo Mission Project for their support and carrying this work through. We also thank A. Lacis and J. Hansen for leadership during the early phases of the PPR instrument development, E. Russell for design work, J. Ferrier for maintaining a radiometric calibration scheme, and H. Peiris and C. Connor for their work in processing the data.

4 September 1996; accepted 26 September 1996

Galileo Plasma Wave Observations in the Io Plasma Torus and Near Io

D. A. Gurnett, W. S. Kurth, A. Roux, S. J. Bolton, C. F. Kennel

The Galileo plasma wave instrument detected jovian radio emissions, narrowband upper hybrid waves, and whistler-mode emissions during the inbound pass through the Io torus. The upper hybrid waves provided an accurate profile of electron density through the Io torus and in the vicinity of Io. These measurements show that the torus density has increased by about a factor of 2 since the Voyager 1 flyby in 1979. A well-defined peak in the electron density was observed in the wake of Io, with densities as high as about 4 × 10^4 per cubic centimeter.

Here we give an overview of results from the Galileo plasma wave instrument during the inbound pass through the Io torus on 7 December 1995, including the flyby of Io. The plasma wave subsystem (PWS) was designed to measure the spectrum of plasma waves and radio emissions over a frequency range from 5 Hz to 5.6 MHz (*1*). During the inbound pass, magnetospheric particle and fields data were obtained from 15:21 to 18:25 UT (universal time). This period includes the Io closest approach (CA) at 17:46 UT. Intense jovian radio emissions called hectometric radiation (*2*, *3*) are evident in the electric field spectrogram at frequencies above 1 MHz (Fig. 1). At somewhat lower frequencies, an intense narrowband emission line extends across the electric field spectrogram at frequencies of a few hundred kilohertz. Narrowband emissions of this type are observed in the magnetospheres of Earth (*4*) and the outer planets (*2*, *5*) and are caused by electrostatic waves at the upper hybrid frequency f_{UH}. At even lower frequencies, an intense band of noise extends across both the electric-field and the magnetic-field spectrograms in the frequency range from a few hertz to a few kilohertz (Fig. 1). The presence of a magnetic component in this frequency range, between the proton cyclotron frequency (~10 to 30 Hz) and the electron cyclotron frequency (~20 to 60 kHz), uniquely identifies this noise as whistler-mode emissions (*6*). The same type of noise was detected during the Voyager 1 pass through the Io torus (*7*); however, Voyager did not have a magnetic antenna, so a unique mode identification was not possible. Whistler-mode emissions of this type are believed to be generated by energetic radiation-belt electrons (*8*).

Considerable variability exists in the intensity of the whistler-mode noise (Fig. 1). Numerous steplike enhancements lasting several minutes can be seen, for example, from 17:09 to 17:15 UT. Comparisons with data from the energetic-particle detector (EPD) show that these enhancements are closely correlated with increases in the intensity of trapped 15- to 300-keV electrons (*9*). Large variations in the spectrum and intensity of the low-frequency electric and magnetic noise can also be seen near the point of closest approach to Io. A brief, intense burst of broadband electric and magnetic field noise in the downstream wake of Io, from about 17:45:30 to 17:47:30 UT, corresponds almost exactly with the region where the EPD instrument detected an intense bidirectional field-aligned beam of 15- to 100-keV electrons (*10*), apparently accelerated in the vicinity of Io.

The emission line at f_{UH} provides an accurate method of determining the local electron density. The upper hybrid frequency is given by $f_{UH} = (f_p^2 + f_c^2)^{1/2}$

D. A. Gurnett and W. S. Kurth, Department of Physics and Astronomy, University of Iowa, Iowa City, IA 52242, USA.
A. Roux, Centre d'Etudes des Environnements Terrestre et Planetaires, Universite Versailles Saint Quentin, 10/12 Avenue de l'Europe, 78140 Velizy, France.
S. J. Bolton, Jet Propulsion Laboratory, 4800 Oak Grove Drive, Pasadena, CA 91109, USA.
C. F. Kennel, Office of the Chancellor, University of California, Los Angeles, CA 90095, USA.